Radio Science

RESEARCH ARTICLE
10.1029/2023RS007776

Four-Beams-Reconfigurable Circular-Ring Array Antennas for Monopulse Radar Applications

Giada M. Battaglia[1,2], Tommaso Isernia[1,2], Roberta Palmeri[1,2,3], and Andrea F. Morabito[1,2]

[1]DIIES Department, Università Mediterranea of Reggio Calabria, Reggio Calabria, Italy, [2]Consorzio Nazionale Interuniversitario per le Telecomunicazioni (CNIT), Parma, Italy, [3]Institute for the Electromagnetic Sensing of the Environment of the National Council of Research (IREA-CNR), Napoli, Italy

Key Points:

- Phase-only reconfigurable circular-ring arrays can be exploited as effective monopulse antennas
- Orbital Angular Momentum vortex beams increase precision pointing
- Convex Programming can maximize performance of reconfigurable arrays

Correspondence to:

A. F. Morabito,
andrea.morabito@unirc.it

Citation:

Battaglia, G. M., Isernia, T., Palmeri, R., & Morabito, A. F. (2023). Four-beams-reconfigurable circular-ring array antennas for monopulse radar applications. *Radio Science*, *58*, e2023RS007776. https://doi.org/10.1029/2023RS007776

Received 26 MAY 2023
Accepted 12 AUG 2023

Abstract We propose a new approach to the mask-constrained power synthesis of reconfigurable circular-ring array antennas for monopulse radar applications. By resorting to Orbital Angular Momentum vortex beams, and without increasing either the complexity of the beam forming network or the signal processing times with respect to the state-of-art solutions, the proposed method allows improving the precision pointing with respect to usual techniques. The overall synthesis is cast as a Convex Programming optimization problem aimed at reducing as much as possible the number of control points of the array, and it is tested in relevant application scenarios.

Plain Language Summary A new antenna-design method is presented in order to enhance the target localization accuracy of monopulse radars. The synthesis procedure is cast as a Convex Programming problem in the case of reconfigurable circular arrays.

1. Introduction

Monopulse radars are usually conceived as antennas able to generate a pencil beam and two difference beams. In particular, the pencil beam (also called "sum" pattern) is used in the transmitting mode, while the difference beams (also referred to as "delta" patterns) are used in the receiving mode and are respectively generated on the elevation (up-down) and traverse (left-right) directions. By virtue of this feature, these systems are able to determine the range and direction from a single signal pulse (Sherman, 1984).

When monopulse radars are realized as fixed-geometry planar array antennas, the array layout is divided into four independent quadrants, and the radiation behavior is reconfigured from the sum beam to the difference beams (and vice-versa) by adjusting the elements' amplitude and phase excitations (Rocca & Morabito, 2015). In order to simplify this operation as well as the required beam forming network (BFN), several techniques have been proposed in order to minimize the portion of the excitation amplitudes which must be changed in order to grant reconfigurability or, better to say, to maximize the excitation amplitudes shared amongst the different radiation modalities—see (Bui et al., 2021; Ferrando-Rocher et al., 2023; Heidari et al., 2023; Morabito & Rocca, 2010; Shirkolaei & Ghalibafan, 2021; Shirkolaei & Jafari, 2020). These techniques often exploit the fact that, in both cases of sum and difference patterns, the source exhibits a decaying behavior at the outer part of the aperture (Bayliss, 1968; Elliott, 1976; McNamara, 1993).

As far as difference patterns generated by planar arrays are concerned, the most common techniques produce fields exhibiting an antisymmetric behavior and hence power patterns having a line of zeroes passing through boresight (Bucci et al., 2005; Fan et al., 2020; Rocca & Morabito, 2015). Therefore, while requiring a simple BFN and providing an easy and fast commutation between the sum and difference modes, these systems may imply ambiguities (and hence loss of resolution) in the azimuth direction when the difference pattern comes from elevation and vice versa.

To counteract such an issue, exploitation of Orbital Angular Momentum (OAM) vortex beams has been recently proposed (Battaglia et al., 2023b; Kou & Yu, 2022; Yu & Kou, 2022). In fact, this kind of fields generates a power pattern having a circularly-symmetric behavior as well as a null at boresight or, better to say, a circularly-symmetric difference pattern.

Notably, the single isolated null of the field in the target direction allows improving the target localization accuracy with respect to common techniques leading to lines of power-pattern zeroes in the spectral plane. On the other side,

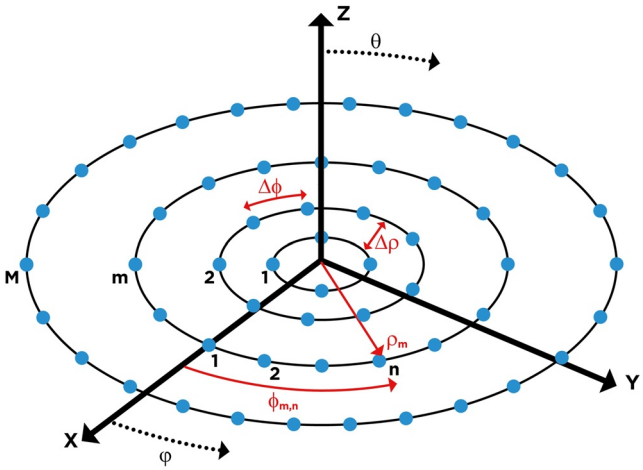

Figure 1. Geometry of the ring array exploited to generate the four reconfigurable beams. This kind of layout is renowned for its advantages over square and rectangular arrays (Bucci et al., 2010).

while the traditional difference beams can quickly determine the azimuth and elevation angles of the target through a couple of one-dimensional scans, the OAM difference patterns do not allow measuring the azimuth or elevation angles independently. Rather, they require a two-dimensional scanning of the entire spectral domain, which may increase the time for locating the target (Battaglia et al., 2023b).

Taking into account all these considerations, in the attempt of bringing at the same time all the advantages of both the classical methods and the modern OAM-based design techniques, this paper introduces a new approach to the synthesis of reconfigurable circular-ring arrays for monopulse radar applications. In particular, the aim is that of generating, by changing the excitation phases plus a portion of the excitation amplitudes, one pencil beam plus three difference patterns. Among the three difference patterns, two are conceived as "classical" antisymmetric fields and are meant to be used for the target localization respectively in the azimuth and elevation directions, while the third one is an OAM difference beam having a single isolated null in the target direction. By so doing, it will be possible to use the first two difference patterns in order to quickly identify the azimuth and elevation angles of the target through a couple of fast one-dimensional scans and, then, to exploit the OAM difference field (only in the target region extracted by means of the two previously-used difference patterns) in order to increase the localization accuracy.

It is worth noting that, besides being able to improve the performance of OAM difference patterns and hence the target localization accuracy, the proposed technique is the first and only one capable of addressing the synthesis of reconfigurable arrays able to simultaneously generate four mask-constrained power patterns for monopulse radar communications using a single antenna layout and sharing an arbitrary number of excitation amplitudes.

In the following, the developed synthesis approach is presented in Section 2 and assessed in Section 3. Conclusions follow.

2. Statement and Optimal Solution of the Synthesis Problem

The goal of the synthesis approach is to design a reconfigurable circular-ring array able to generate four far field distributions pertaining to different operation modes, that is, one pencil beam (say F_{Σ}), one OAM beam (say F_{OAM}), one difference beam along the elevation direction (say $F_{\Delta 1}$), and one difference beam along the azimuth direction (say $F_{\Delta 2}$). The approach has been engineered in such a way to grant an easy adjustability of the antenna as well as a minimization of the required control points.

To present the design procedure, let us consider a circular-ring array whose radiating elements are arranged on M concentric rings having radii $\rho_1,\ldots,\rho_M$ and denote by N_m, for $m = 1,\ldots,M$, the number of elements located on the m-th ring. For the sake of simplicity, let us suppose that both the spacing between the different rings (say $\Delta\rho$) as well as the spacing between neighboring elements located on the same ring (say $\Delta\phi$) are constant all over the array layout (see Figure 1). Finally, for $n = 1,\ldots,N_m$ (with $m = 1,\ldots,M$) let us denote with $(\rho_m, \phi_{m,n})$ the radial and azimuth coordinates of the n-th element belonging to the m-th ring.

It is worth noting that the array shown in Figure 1, which is meant to work as a monopulse antenna, can be easily fed by using, for instance, the techniques discussed in Leonardi et al. (2014), Mohammadi et al. (2009), and Mohammadi and Kashani (2009).

By resorting to the Active Element Patterns defined as in Morabito, Di Carlo, et al. (2019), the devised synthesis procedure can be applied whatever the kind of radiating elements and can take into account mutual-coupling and mounting-platform effects. However, to keep things simple, from now on the far field generated by the array will be expressed as the array factor. This assumption does not entail any loss of generality, and it is the same of as the one made in the recent contributions (Kou & Yu, 2022; Yu & Kou, 2022) dealing with same kind of array geometry in order to generate OAM fields. Therefore, by denoting with $\beta = 2\pi/\lambda$ the wavenumber (λ being the

operating wavelength), and expressing as $u = \beta\sin\theta\cos\varphi$ and $v = \beta\sin\theta\sin\varphi$ the usual spectral variables (θ and φ respectively denoting the array-aperture elevation and azimuth angles), the far field distributions pertaining to the four operation modes are expressed as follows:

$$F_{\Sigma}(u, \mathrm{v}) = \sum_{m=1}^{M}\sum_{n=1}^{N_m} I_{\Sigma m,n} e^{j\left(u\rho_m \cos\phi_{m,n} + v\rho_m \sin\phi_{m,n}\right)} \tag{1a}$$

$$F_{\mathrm{OAM}}(u, \mathrm{v}) = \sum_{m=1}^{M}\sum_{n=1}^{N_m} I_{\mathrm{OAM}m,n} e^{j\left(u\rho_m \cos\phi_{m,n} + v\rho_m \sin\phi_{m,n}\right)} \tag{1b}$$

$$F_{\Delta 1}(u, \mathrm{v}) = \sum_{m=1}^{M}\sum_{n=1}^{N_m} I_{\Delta 1\, m,n} e^{j\left(u\rho_m \cos\phi_{m,n} + v\rho_m \sin\phi_{m,n}\right)} \tag{1c}$$

$$F_{\Delta 2}(u, \mathrm{v}) = \sum_{m=1}^{M}\sum_{n=1}^{N_m} I_{\Delta 2 m,n} e^{j\left(u\rho_m \cos\phi_{m,n} + v\rho_m \sin\phi_{m,n}\right)} \tag{1d}$$

where $I_{\Sigma m,n}$, $I_{\mathrm{OAM}m,n}$, $I_{\Delta 1\, m,n}$, and $I_{\Delta 2 m,n}$ denote, for each of the corresponding radiation mode, the complex excitation of the nth element belonging to the m-th ring of the array. The latter, in turn, by respectively denoting with γ and A the phase and the amplitude of each excitation and assuming, as made in Battaglia et al. (2023b), that all elements belonging to the same ring have the same excitation amplitude, can be expressed $\forall(m, n)$ as follows:

$$I_{\Sigma m,n} = A_{\Sigma m} e^{j\gamma_{\Sigma m,n}} \tag{2a}$$

$$I_{\mathrm{OAM}m,n} = A_{\mathrm{OAM}m} e^{j\gamma_{\mathrm{OAM}m,n}} \tag{2b}$$

$$I_{\Delta 1\, m,n} = A_{\Delta 1\, m} e^{j\gamma_{\Delta 1\, m,n}} \tag{2c}$$

$$I_{\Delta 2 m,n} = A_{\Delta 2 m} e^{j\gamma_{\Delta 2 m,n}} \tag{2d}$$

With respect to the case where different excitation amplitudes are allowed for elements belonging to the same ring, this choice may lead to a reduction of the degrees of freedom of the synthesis and hence to a possible decrease of the overall radiation performance. On the other side, it also allows dramatically reducing the number of required amplifiers and, hence, the complexity and weight of the BFN. Furthermore, it grants an easy adjustability of the antenna configuration and considerably reduces the number of unknowns of the optimization problem presented in the following (which, for instance, decreases from $\sum_{m=1}^{M} N_m$ to M in case a phase-only reconfigurable array is sought), with the inherent advantages in terms of efficiency and computational time.

The synthesis performed as follows.

As a first step, a suitable array layout for the scenario at hand is identified. This is done by setting the values of M, $\Delta\rho$, and $\Delta\phi$ according to the requirements in terms of array size and overall number of elements, and also by taking into account some desired parameters for the different radiation patterns as, for instance, their beam-width or divergence angle. Then, we choose the most suitable order of the OAM vortex, say $\hat{\ell}$, by following the guidelines in Battaglia et al. (2023b) and perform an uniform discretization of the spectral variables as $u = [u_1, u_2,\ldots,u_{2Q-1}]$ and $v = [v_1, v_2,\ldots,v_{2Q-1}]$ with $u_1 = v_1 = -\beta$ and $u_{2Q-1} = v_{2Q-1} = \beta$. In particular, a sampling rate larger than the Nyquist one given in Bucci et al. (1998) is recommended and, in order to ensure a sufficiently-fine discretization, we set $Q = \lceil 10\rho_M/\lambda \rceil$. This is coherent with the choice we made in other applications (Morabito, Palmeri, et al., 2019; Palmeri et al., 2019) and allows identifying as $(u_Q, v_Q) = (0, 0)$ the origin of the spectral plane which, in turn, is required to compute the fields' slope when the target direction is set as the boresight (as it will be assumed from now on).

Once the array geometry, the most suitable order of the OAM vortex, and the discretized spectral variables are set, the elements' excitation phases are chosen as follows:

$$\gamma_{\Sigma m,n} = 0 \quad \forall m, n \tag{3a}$$

$$\gamma_{\mathrm{OAM}m,n} = -\hat{\ell}\,\phi_{m,n} \quad \forall m, n \tag{3b}$$

$$\gamma_{\Delta 1_{m,n}} = \begin{cases} \pi & if\ \pi/2 < \phi_{m,n} \le 3\pi/2 \\ 0 & \text{otherwise} \end{cases} \tag{3c}$$

$$\gamma_{\Delta 2_{m,n}} = \begin{cases} \pi & if\ \pi < \phi_{m,n} \le 2\pi \\ 0 & \text{otherwise} \end{cases} \tag{3d}$$

In fact, Equation 3a follows the rules in Bucci, Isernia, and Morabito (2009), Bucci, Isernia, Morabito, Perna, and Pinchera (2009) where it is shown that the optimal aperture distribution for a pencil beam with maximum directivity is real, Equation 3b complies with (Battaglia et al., 2023b), and Equations 3c and 3d allow generating, by virtue of the symmetry of the array layout, the two difference patterns (Rocca & Morabito, 2015). It is worth noting that a-priori choosing the excitation phases is strictly required in order to make "convex" the constraints on excitation amplitudes which, in turn, is necessary in order to enable the optimal synthesis of phase-only reconfigurable arrays.

Once the optimal excitation phases are selected, optimizing the excitation amplitudes allows identifying the final values of the complex excitations (2). This is done by solving the following optimization problem in the (real) unknowns $A_{\Sigma 1}$, $A_{\mathrm{OAM}1}$, $A_{\Delta 1 1}$, $A_{\Delta 2 1}$, …, $A_{\Sigma M}$, $A_{\mathrm{OAM}M}$, $A_{\Delta 1 M}$, $A_{\Delta 2 M}$:

$$\min -\left\{ \begin{array}{c} \alpha_\Sigma Re\left[F_\Sigma(u_Q, v_Q)\right] + \alpha_{\mathrm{OAM}} Re\left[\frac{F_{\mathrm{OAM}}(u_{Q+1}, v_Q) - F_{\mathrm{OAM}}(u_Q, v_Q)}{u_{Q+1} - u_Q}\right] + \\ + \alpha_{\Delta 1} Im\left[\frac{F_{\Delta 1}(u_{Q+1}, v_Q) - F_{\Delta 1}(u_Q, v_Q)}{u_{Q+1} - u_Q}\right] + \alpha_{\Delta 2} Im\left[\frac{F_{\Delta 2}(u_Q, v_{Q+1}) - F_{\Delta 2}(u_Q, v_Q)}{v_{Q+1} - v_Q}\right] \end{array} \right\} \tag{4}$$

subject to:

$$Im\left[F_\Sigma(u_Q, v_Q)\right] = 0 \tag{5a}$$

$$Im\left[\frac{F_{\mathrm{OAM}}(u_{Q+1}, v_Q) - F_{\mathrm{OAM}}(u_Q, v_Q)}{u_{Q+1} - u_Q}\right] = 0 \tag{5b}$$

$$Re\left[\frac{F_{\Delta 1}(u_{Q+1}, v_Q) - F_{\Delta 1}(u_Q, v_Q)}{u_{Q+1} - u_Q}\right] = 0 \tag{5c}$$

$$Re\left[\frac{F_{\Delta 2}(u_Q, v_{Q+1}) - F_{\Delta 2}(u_Q, v_Q)}{v_{Q+1} - v_Q}\right] = 0 \tag{5d}$$

$$|F_\Sigma(u, v)|^2 \le UB_\Sigma(u, v) \quad \forall (u, v) \in \Omega_\Sigma \tag{6a}$$

$$|F_{\mathrm{OAM}}(u, v)|^2 \le UB_{\mathrm{OAM}}(u, v) \quad \forall (u, v) \in \Omega_{\mathrm{OAM}} \tag{6b}$$

$$|F_{\Delta 1}(u, v)|^2 \le UB_{\Delta 1}(u, v) \quad \forall (u, v) \in \Omega_{\Delta 1} \tag{6c}$$

$$|F_{\Delta 2}(u, v)|^2 \le UB_{\Delta 2}(u, v) \quad \forall (u, v) \in \Omega_{\Delta 2} \tag{6d}$$

$$A_{\Sigma_m} \ge 0 \quad \forall m \tag{7a}$$

$$A_{\mathrm{OAM}_m} \ge 0 \quad \forall m \tag{7b}$$

$$A_{\Delta 1_m} \ge 0 \quad \forall m \tag{7c}$$

$$A_{\Delta 2_m} \ge 0 \quad \forall m \tag{7d}$$

$$A_{\Sigma_m} = A_{\mathrm{OAM}_m} = A_{\Delta 1_m} = A_{\Delta 2_m} \quad \forall m \ge M_R \tag{8}$$

where M_R is an integer such that $1 \le M_R \le M$, while Re and Im respectively denote the real and imaginary parts.

Details and motivations about the above problem formulation are given in the follows.

By paralleling (Bucci et al., 2005; Isernia & Panariello, 1998), the objective function (4) (where α_{Σ}, α_{OAM}, $\alpha_{\Delta 1}$, $\alpha_{\Delta 2}$ are real and positive numerical constants chosen by the user) subject to constraints (5) allows maximizing, in the target direction, the weighted sum of the square amplitude of F_{Σ} plus the "discretized" slopes of F_{OAM}, $F_{\Delta 1}$, and $F_{\Delta 2}$. In particular, since the problem formulation is given in terms of array factors, constraints (5) take advantage of the fact that, by virtue of the general theory about oddness and evenness of Fourier Transform (Bracewell, 1999), for an array with symmetric elements' locations, real and symmetric excitations (as the ones entailed by Equation 3a) are expected to lead to real and symmetric far field distributions, while real and antisymmetric excitations (as entailed by Equations 3c and 3d) are expected to lead to imaginary and antisymmetric far field distributions.

While the amplitude of the pencil beam as well as the slope of the difference beams are maximized in the target direction, constraints (6) allow keeping under control the sidelobe level (SLL) of the four power patterns by enforcing that they do not exceed the (real and positive) upper bound functions UB_{Σ}, UB_{OAM}, $UB_{\Delta 1}$, and $UB_{\Delta 2}$ in the regions of the spectral plane respectively identified by Ω_{Σ}, Ω_{OAM}, $\Omega_{\Delta 1}$, and $\Omega_{\Delta 2}$.

Finally, constraints (7) are consistent with the fact that the (real) unknowns $A_{\Sigma 1}$, $A_{\mathrm{OAM}\,1}$, $A_{\Delta 1\,1}$, $A_{\Delta 2\,1}$, …, $A_{\Sigma M}$, $A_{\mathrm{OAM}\,M}$, $A_{\Delta 1\,M}$, $A_{\Delta 2\,M}$ are meant to be excitation amplitudes, and constraint (8) allows significantly simplifying the BFN by enforcing that the excitation amplitudes pertaining to the four power patterns are equal to each other in the outer part of the array layout. This constraint takes advantage of the decreasing behavior typically shared by the reference sources generating sum and difference patterns (Morabito & Rocca, 2010), and leads to a "phase-only reconfigurable" array (where only the excitation phases must be changed in order to switch from a radiation modality to another) provided that $M_R = 1$ is adopted. In any case, the percentage P of excitation amplitudes shared by the four operating modes will be given by:

$$P = \frac{\sum_{m=M_R}^{M} N_m}{\sum_{m=1}^{M} N_m} \tag{9}$$

As a crucial feature of the overall formulation (4)–(8), it is worth noting that Equations (4), (5), (7), and (8) are linear forms of the unknowns, while (6) are positive semidefinite quadratic forms. Therefore, the overall optimization problem is a Convex Programming (CP) one where the solution set is unique (provided that it exists) and hence it is also the globally-optimal one. This makes possible to quickly identifying the best array configuration without recurring to computationally-expensive global-optimization algorithms like the one recently used in M. Li et al. (2021) for the design of sum and difference patterns and the ones usually exploited in order to keep under control the SLL of OAM beams (Qin et al., 2017; Q. Li et al., 2018, 2019).

As a final comment concerning the overall approach, it is worth noting that, by virtue of constraints (5), one can also change the objective function (4) by pursuing the minimization of only one, two, or three of its addenda while enforcing, as a set of linear constraints, that the remaining ones are equal to properly-chosen constants. This case, however, is not explored here since the procedure has been devised as a "fair treatment" of all four beams. For this reason, $\alpha_{\Sigma} = \alpha_{\mathrm{OAM}} = \alpha_{\Delta 1} = \alpha_{\Delta 2} = 1$ will be assumed from now on.

3. Numerical Assessment

As a representative sample of the numerical experiments performed in order to test the proposed approach, we report in the following the outcomes of the synthesis of a phase-only reconfigurable array (Section 3.1) plus a comparison with a very recent work that used OAM beams to maximize the performance of a single difference pattern (Section 3.2).

All numerical examples have been performed by setting the target direction as $\theta = 0°$ and using a generic working frequency, so that all the antennas' size and the elements spacing are expressed as a function of λ. We also set $\hat{\ell} = 1$ by following the guidelines in Battaglia et al. (2023b), and discretized the spectral variables u and v into $2Q - 1 = 201$ equispaced samples (which systematically results larger even than the value provided by the rule $Q = \lceil 10\rho_M/\lambda \rceil$ described in the previous Section).

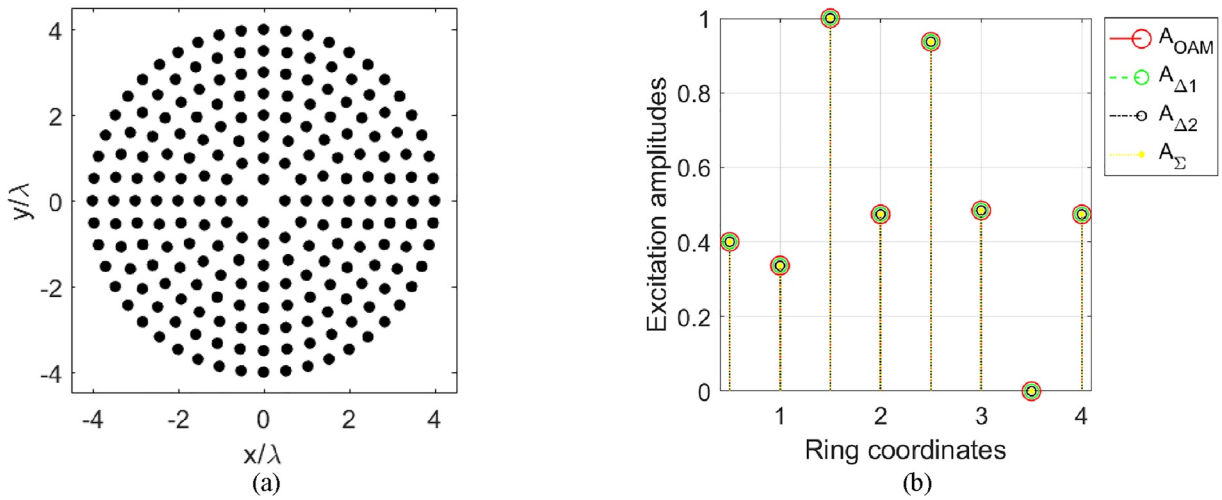

Figure 2. Phase-only reconfigurable array composed of 208 elements [subplot (a)] and synthesized excitation amplitudes [subplot (b)]. The rings have coordinates $\{0.5, 1.0, 1.5, 2.0, 2.5, 3.0, 3.5, 4.0\}\lambda$. The number of antennas per ring is equal to $\{4, 12, 16, 24, 28, 36, 40, 48\}$. The excitation amplitudes are as follows: $A_{OAM} = A_{\Delta 1} = A_{\Delta 2} = A_{\Sigma} = \{0.400, 0.337, 1.000, 0.474, 0.937, 0.484, 0.000, 0.474\}$.

As far as the upper bound on the sidelobes' maximum amplitude is concerned, we set $UB_{\Sigma} = UB_{OAM} = UB_{\Delta 1} = UB_{\Delta 2} = 0$ dB and adopted a proper shape of Ω_{Σ}, Ω_{OAM}, $\Omega_{\Delta 1}$, and $\Omega_{\Delta 2}$. In particular, due to the expected circular footprint of $|F_{\Sigma}(u, v)|^2$ and $|F_{OAM}(u, v)|^2$, Ω_{Σ} and Ω_{OAM} have been set as two circles having a radius in the spectral plane respectively equal to R_{Σ} and R_{OAM}. Furthermore, due to the typical footprints of $|F_{\Delta 1}(u, v)|^2$ and $|F_{\Delta 2}(u, v)|^2$, we found it convenient to set $\Omega_{\Delta 1}$ and $\Omega_{\Delta 2}$ as two ellipses both having the major axis equal to R_{OAM} and the minor axis equal to $R_{OAM}/2$ in the spectral plane.

Finally, from now on, the SLL is meant as the difference between the maximum amplitude (in dB) of the sidelobes and the maximum amplitude (in dB) of the main beam of the power pattern. For each numerical experiments, the divergence angle θ_D (meant as the elevation coordinate where any difference pattern attains its maximum amplitude) is also reported for F_{OAM}, $F_{\Delta 1}$, and $F_{\Delta 2}$, while the half-power beamwidth (HPBW) is reported for F_{Σ}.

3.1. Synthesis of Phase-Only Reconfigurable Arrays

As a first interesting application, we used the presented approach in order to design a phase-only reconfigurable array able to generate the four power patterns F_{Σ}, F_{OAM}, $F_{\Delta 1}$, $F_{\Delta 2}$ and to switch from any modality to another one by changing just the excitations' phase. In this case, the four radiation modalities share the array layout as well as the 100% of the excitation amplitudes, which minimize the number of control points as well as the complexity, weight, and cost of the BFN (Morabito & Rocca, 2010).

Notably, apart from the present work, no contributions are available today in the open literature able to address the joint generation of the above four patterns through phase-only reconfigurable arrays.

To define the array layout, we set $M = 8$ and $\Delta\rho = \Delta\phi = 0.5\lambda$. Then, in order to further simplify the BFN as well as the possible fabrication of the antenna, we enforced a quadrantal symmetry of the layout by rounding N_m, for $m = 1,\ldots,M$, in order to get a number of elements located on each ring that is a multiple of 4. In fact, in this way the array can be conceived as the union of four subarrays equal to each other in terms of elements' location (see Figure 2). This choice led to an overall number of elements equal to 208.

As far as the radiation constraints are concerned, we set $R_{\Sigma} = 2$ and $R_{OAM} = 1.2$. The radiation pattern of each element has been chosen as $\cos\theta$ and, in order to get the desired phase-only reconfigurability, we set $M_R = 1$.

The array layout and the synthesized excitation amplitudes are shown in Figure 2, whose caption also reports the ring coordinates, the number of elements per ring, and the values of the achieved excitation amplitudes. The four corresponding radiation patterns are shown in Figures 3–6. Notably, while sharing all the excitation amplitudes,

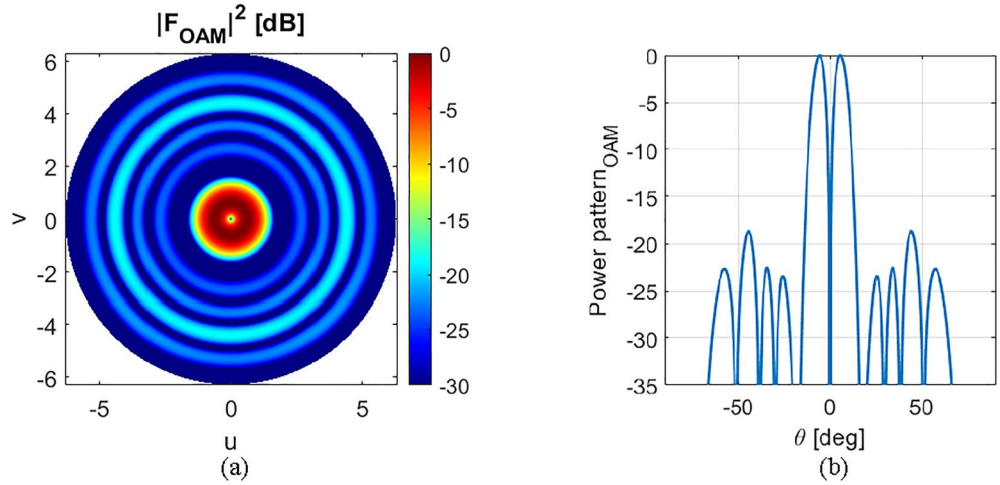

Figure 3. Design of a phase-only reconfigurable array: synthesized OAM difference power pattern [subplot (a)] and its 1-D cut for $u = 0$ [subplot (b)].

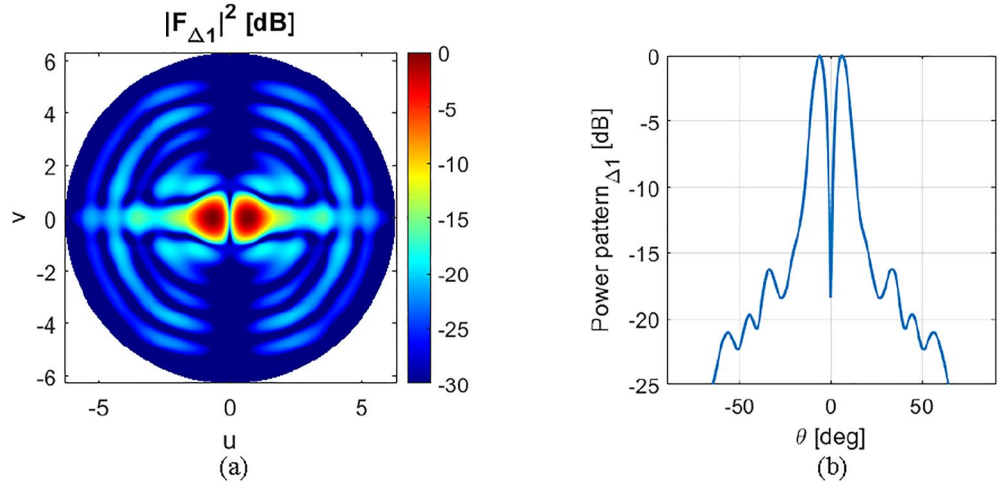

Figure 4. Design of a phase-only reconfigurable array: synthesized elevation difference power pattern [subplot (a)] and its 1-D cut for $u = 0$ [subplot (b)].

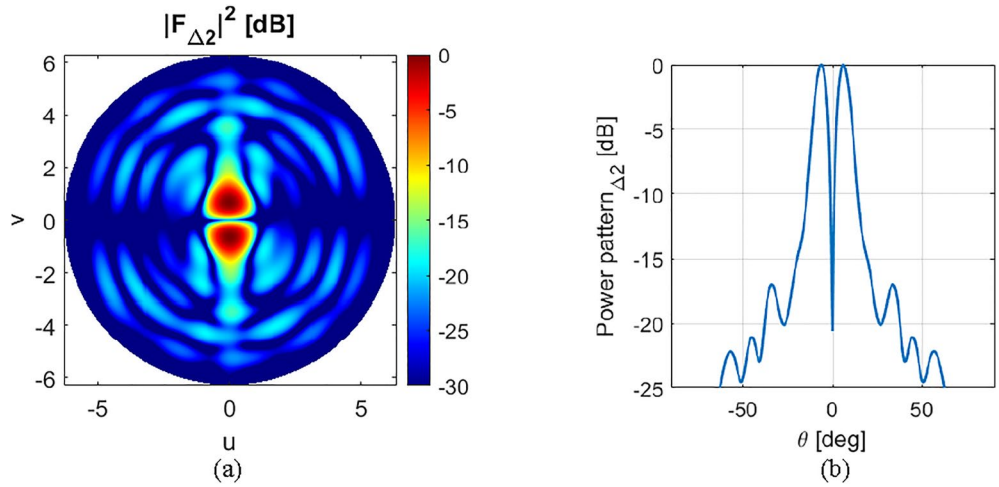

Figure 5. Design of a phase-only reconfigurable array: synthesized azimuthal difference power pattern [subplot (a)] and its 1-D cut for $v = 0$ [subplot (b)].

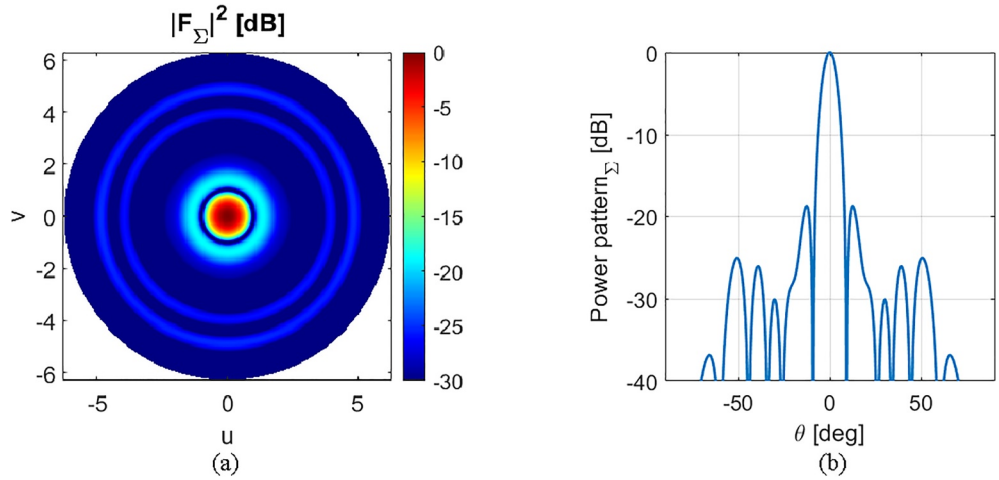

Figure 6. Design of a phase-only reconfigurable array: synthesized sum power pattern [subplot (a)] and its 1-D cut for $u = 0$ [subplot (b)].

the achieved solutions provide SLL = −19 dB and $\theta_D = \pm 5.7°$ for F_{OAM}, SLL = −16 dB and $\theta_D = \pm 6.1°$ for $F_{\Delta 1}$ and $F_{\Delta 2}$, SLL = −19 dB and HPBW = ±3.8° for F_{Σ}. The achieved results confirm the capabilities and effectiveness of the proposed approach in the design circular-ring phase-only reconfigurable arrays.

3.2. Comparison With a Recently Published, Powerful Technique

As a second set of numerical experiments, we thought it appropriate to compare the proposed approach with a recently-published powerful technique. Since no procedures are available today to simultaneously generate, how the proposed method is able to do, the four reconfigurable beams described in Section 2, we have been forced to compare our approach to a technique able to generate only the OAM difference pattern. In particular, we report in the following the outcomes of the comparison with the method recently published in Kou and Yu (2022) which appears being the most powerful one available today for maximizing the performance of F_{OAM}. As it will be shown, despite being able to simultaneously generate not only F_{OAM} but also F_{Σ}, $F_{\Delta 1}$, and $F_{\Delta 2}$, the technique herein proposed turned out being able to achieve in terms of F_{OAM} better performances than the one shown in Kou and Yu (2022).

Coming to details (Kou & Yu, 2022), is a very recent work where OAM vortices are exploited to improve the performance of difference patterns and, in particular, the synthesis is aimed at minimizing the sidelobe level. The best result reported by the authors is a power pattern having a SLL = −36.44 dB, the maximum absolute value located at $\theta = 8.5°$, and the highest-amplitude sidelobe located at $\theta = 27.5°$. This has been done by exploiting the $\ell = 1$ OAM vortex and a circular-ring array composed of 131 isotropic elements, arranged in 6 equispaced rings, with a spacing of 0.5λ between consecutive rings and elements.

For our numerical experiment, we used the same array layout as in Kou and Yu (2022) and hence set $M = 6$ and $\Delta\rho = \Delta\phi = 0.5\lambda$. We also set $R_{\Sigma} = 2$ and $R_{\mathrm{OAM}} = 2.75$, and adopted an isotropic radiation pattern of each element. Finally, by setting $M_R = 6$, we enabled the four radiation modalities to share the excitation amplitude of all elements located on the last ring. In this way, the four modes share almost the 30% of the excitation amplitudes, which is another decisive advantage over the single-beam solution provided by the antenna in Kou and Yu (2022).

The array layout and the synthesized excitation amplitudes are shown in Figure 7, whose caption also reports the ring coordinates, the number of elements per ring, and the excitation values. The four corresponding radiation patterns are shown in Figures 8–11. Notably, while sharing the excitation amplitudes on the last ring, the achieved solution provides SLL = −37 dB and $\theta_D = \pm 8.5°$ for F_{OAM}, SLL = −15 dB and $\theta_D = \pm 7.5°$ for $F_{\Delta 1}$ and $F_{\Delta 2}$, SLL = −30 dB and HPBW = ±6° for F_{Σ}. Therefore, by using the same array layout, the proposed approach provided an OAM difference pattern having a sidelobe level slightly better than (and a divergence angle equal to)

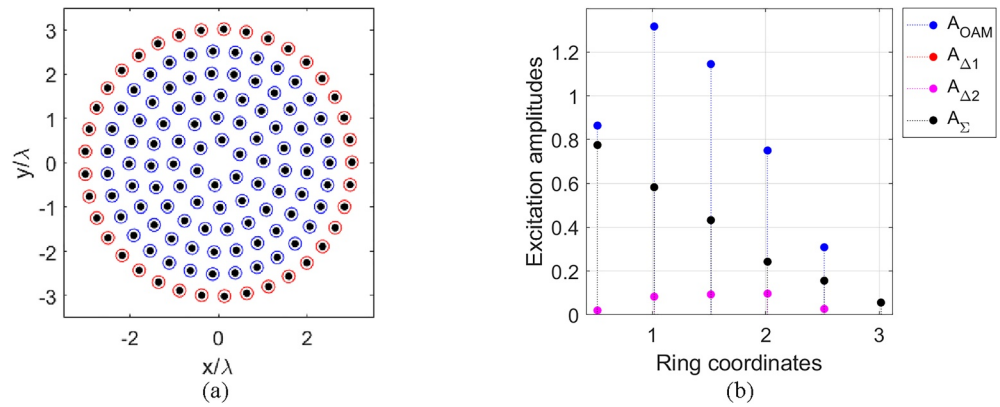

Figure 7. Comparison with (Kou & Yu, 2022) by sharing the array layout plus the 30% of the excitation amplitudes amongst the four radiation modes: array composed of 131 isotropic antennas (where the elements whose excitation amplitude is shared by all function modes are circled in red) [subplot (a)] and synthesized excitation amplitudes [subplot (b)]. The rings have coordinates $\{0.517, 1.017, 1.517, 2.017, 2.517, 3.017\}\lambda$. The number of antennas per ring is equal to $\{6, 12, 19, 25, 31, 37\}$. The excitation amplitudes are as follows: $A_{\mathrm{OAM}} = \{0.864, 1.317, 1.145, 0.750, 0.309, 0.056\}$; $A_{\Delta 1} = A_{\Delta 2} = \{0.020, 0.083, 0.093, 0.097, 0.027, 0.056\}$; $A_{\Sigma} = \{0.775, 0.582, 0.433, 0.243, 0.156, 0.056\}$.

the one of the best solution in Kou and Yu (2022) while still being able to generate the three additional fields by just chancing the excitations of a limited portion of array elements.

Of course, even better performances can be achieved by the proposed approach when removing the constraint about the common excitation amplitudes shared by the four radiation modalities (but still keeping the same array layout for all working modes). In support of this statement, we repeated the numerical experiment above by setting $M_R = 7$, which led to the excitations shown in Figure 12 (whose caption also reports the ring coordinates and the excitation amplitude values of all elements) and to the power patterns shown in Figures 13–16. By keeping, with respect to the previous numerical experiment, the same values of θ_D and HPBW for the four patterns, as well as the same SLL values for $F_{\Delta 1}$ and $F_{\Delta 2}$, the SLL improved from −30 dB to −32 dB for F_{Σ} and from −37 dB to −39 dB for F_{OAM}, further increasing the improvement of performance with respect to (Kou & Yu, 2022) where, despite only one pattern is synthesized, SLL = −36.44 dB has been achieved for F_{OAM}.

The full outcomes of the comparison are shown by Table 1.

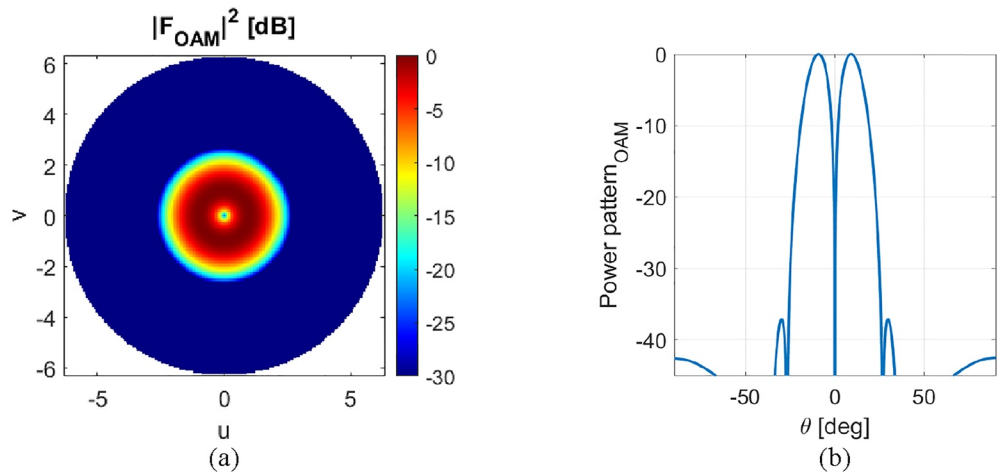

Figure 8. Comparison with (Kou & Yu, 2022) by sharing the array layout plus the 30% of the excitation amplitudes amongst the four radiation modes: synthesized Orbital Angular Momentum difference power pattern [subplot (a)] and its 1-D cut for $u = 0$ [subplot (b)].

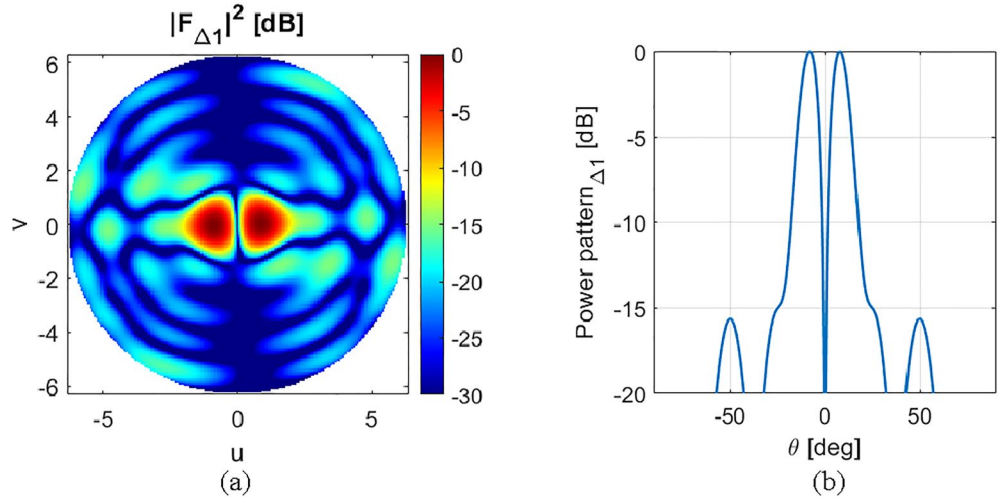

Figure 9. Comparison with (Kou & Yu, 2022) by sharing the array layout plus the 30% of the excitation amplitudes amongst the four radiation modes: synthesized elevation difference power pattern [subplot (a)] and its 1-D cut for $u = 0$ [subplot (b)].

4. Conclusions

A new approach to the mask-constrained power synthesis of concentric ring arrays for monopulse radar applications has been presented and assessed. The developed technique offers the benefits of both the classical methods and the modern OAM-based algorithms available for the synthesis of difference patterns, as well as of the theory for the optimal synthesis of pencil beams. In particular, by resorting to OAM vortex beams, it improves the localization accuracy of conventional difference patterns while roughly preserving the processing times associated to them. An innovative problem formulation in terms of CP optimization has also been given, and the approach has been successfully tested in both cases of phase-only reconfigurable arrays as well as OAM beams granting performances better than the ones of state-of-the-art techniques.

The devised procedure is the first and only one able to design reconfigurable arrays generating four different beams for monopulse communications sharing all elements' locations plus an arbitrary number of excitation amplitudes, thus minimizing the number of required control points.

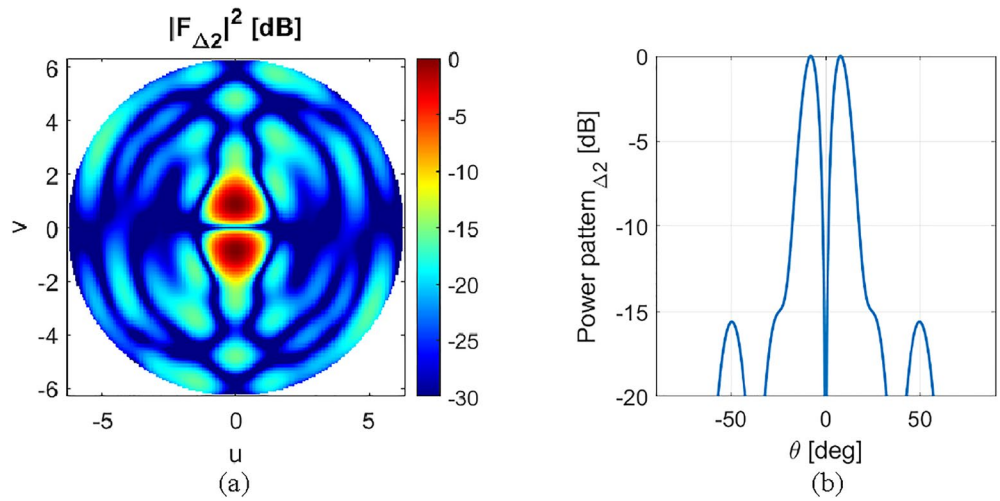

Figure 10. Comparison with (Kou & Yu, 2022) by sharing the array layout plus the 30% of the excitation amplitudes amongst the four radiation modes: synthesized azimuthal difference power pattern [subplot (a)] and its 1-D cut for $v = 0$ [subplot (b)].

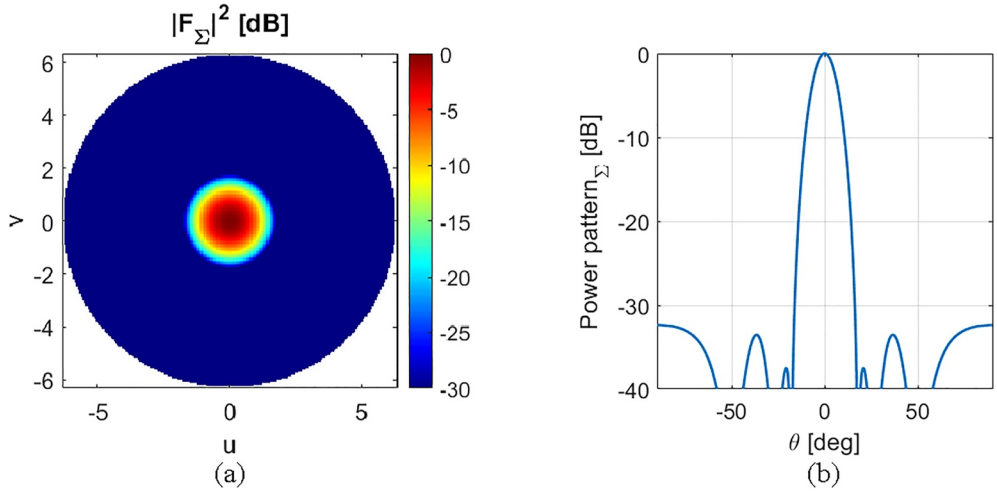

Figure 11. Comparison with (Kou & Yu, 2022) by sharing the array layout plus the 30% of the excitation amplitudes amongst the four radiation modes: synthesized sum power pattern [subplot (a)] and its 1-D cut for $u = 0$ [subplot (b)].

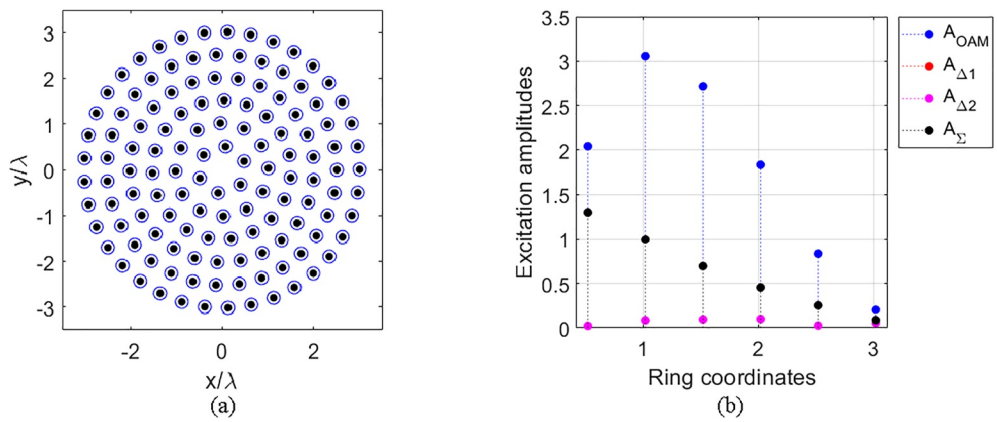

Figure 12. Comparison with (Kou & Yu, 2022) by sharing the array layout amongst the four radiation modes: equispaced array composed of 131 isotropic antennas [subplot (a)] and synthesized excitation amplitudes [subplot (b)]. The rings have coordinates $\{0.517, 1.017, 1.517, 2.017, 2.517, 3.017\}\lambda$. The number of antennas per ring is equal to $\{6, 12, 19, 25, 31, 37\}$. The excitation amplitudes are as follows: $A_{\mathrm{OAM}} = \{2.041, 3.055, 2.715, 1.836, 0.836, 0.208\}$; $A_{\Delta1} = A_{\Delta2} = \{0.023, 0.085, 0.095, 0.099, 0.026, 0.053\}$; $A_\Sigma = \{1.295, 0.997, 0.699, 0.456, 0.257, 0.087\}$.

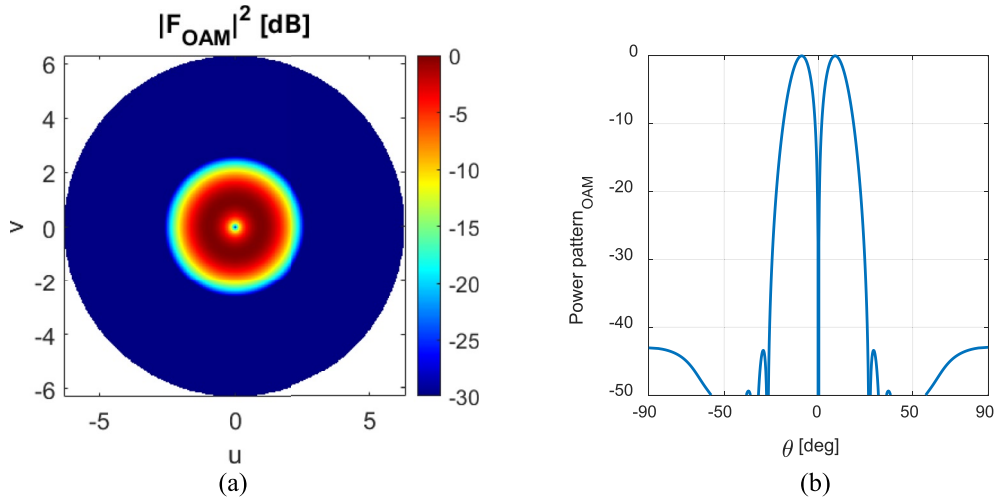

Figure 13. Comparison with (Kou & Yu, 2022) by sharing the array layout amongst the four radiation modes: synthesized OAM difference power pattern [subplot (a)] and its 1-D cut for $u = 0$ [subplot (b)].

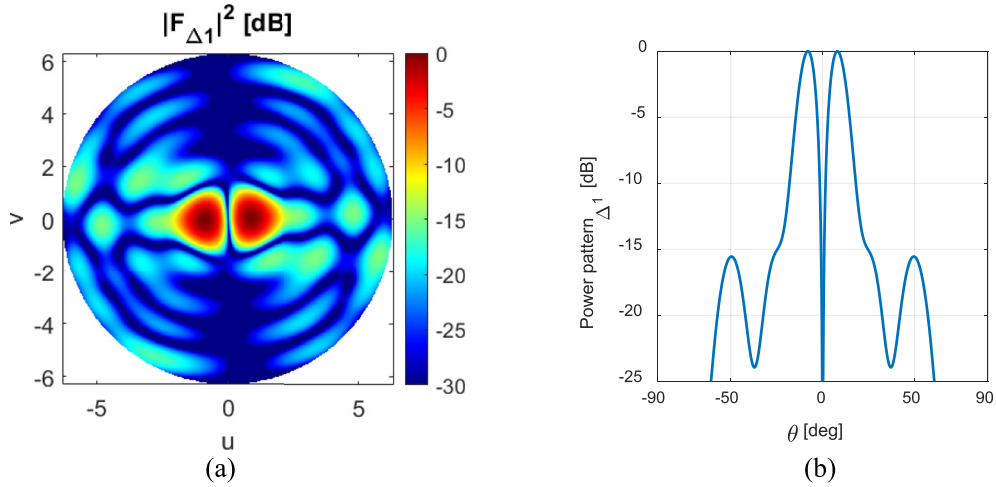

Figure 14. Comparison with (Kou & Yu, 2022) by sharing the array layout amongst the four radiation modes: synthesized elevation difference power pattern [subplot (a)] and its 1-D cut for $u = 0$ [subplot (b)].

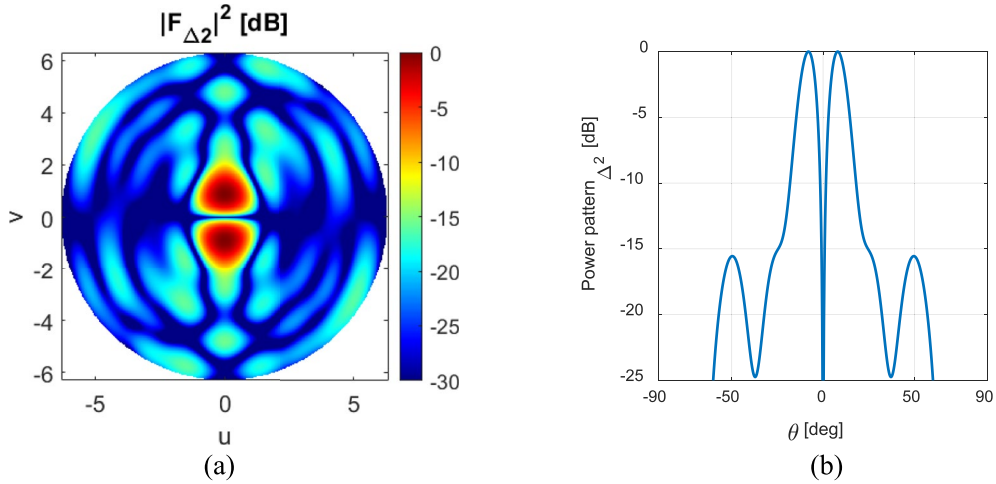

Figure 15. Comparison with (Kou & Yu, 2022) by sharing the array layout amongst the four radiation modes: synthesized azimuthal difference power pattern [subplot (a)] and its 1-D cut for $v = 0$ [subplot (b)].

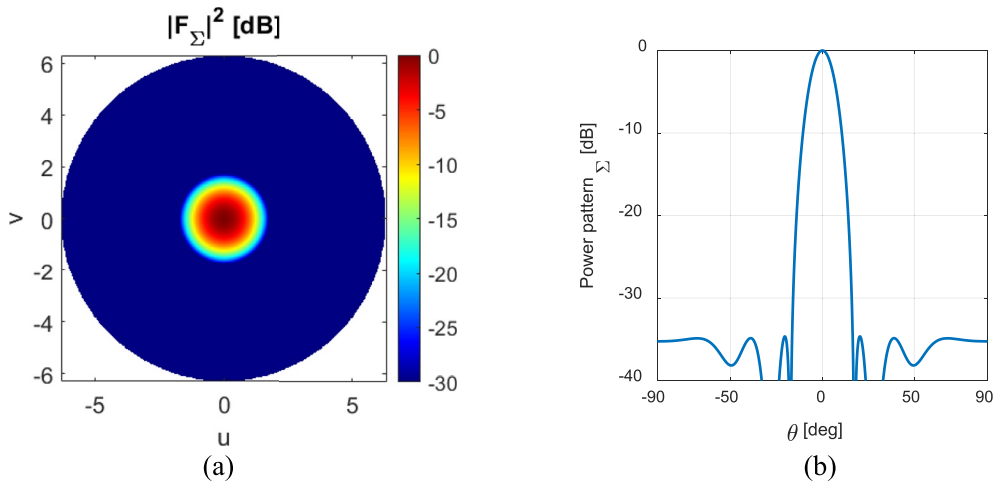

Figure 16. Comparison with (Kou & Yu, 2022) by sharing the array layout amongst the four radiation modes: synthesized sum power pattern [subplot (a)] and its 1-D cut for $u = 0$ [subplot (b)].

Table 1
Comparison of the Proposed Approach With the Technique Recently Published in Kou and Yu (2022)

Performance parameter	Kou and Yu (2022)	This work (NO elements shared by the different modalities)	This work (30% elements shared by the different modalities)
Index of the exploited OAM vortex	1	1	1
Aperture size	3λ	3λ	3λ
Array element pattern	Isotropic	Isotropic	Isotropic
Array number of elements	131	131	131
OAM difference pattern: divergence angle	±8.5°	±8.5°	±8.5°
OAM difference pattern: sidelobe level	−36.44 dB	−39 dB	−37 dB
Azimuth difference pattern: divergence angle	**The beam is not radiated**	±7.5°	±7.5°
Azimuth difference pattern: sidelobe level	**The beam is not radiated**	−15 dB	−15 dB
Elevation difference pattern: divergence angle	**The beam is not radiated**	±7.5°	±7.5°
Elevation difference pattern: sidelobe level	**The beam is not radiated**	−15 dB	−15 dB
Pencil beam: half-power beamwidth	**The beam is not radiated**	±6°	±6°
Pencil beam: sidelobe level	**The beam is not radiated**	−32 dB	−30 dB

Note. For the sake of fairness, since the synthesized power patterns are not circularly symmetric, all SLL values reported by this table are relative to the "worst" beam cut, that is, to the azimuth cut of the field having the highest sidelobes. This means that, along any other azimuth cut, the actual SLL performance is even better than the one reported by the table.

Data Availability Statement

All data and software are available at (Battaglia et al., 2023a).

Acknowledgments
This work has been partially supported by the Italian Ministry of University and Research in part under the project entitled "CYBERPHYSICAL ELECTROMAGNETIC VISION: Context-Aware Electromagnetic Sensing and Smart Reaction" (PRIN 2017HZJXSZ) and in part under the project entitled "TECH4YOU—TECHNOLOGIES FOR CLIMATE CHANGE ADAPTATION AND QUALITY OF LIFE IMPROVEMENT" (CUP H23C22000370006, no. ECS_00000009).

References

Battaglia, G. M., Isernia, T., Palmeri, R., & Morabito, A. F. (2023a). Circular ring arrays exploiting orbital angular momentum [Dataset and Software]. Zenodo. https://doi.org/10.5281/zenodo.7937434

Battaglia, G. M., Isernia, T., Palmeri, R., & Morabito, A. F. (2023b). Synthesis of orbital angular momentum antennas for target localization. *Radio Science*, *58*(2), e2022RS007592. https://doi.org/10.1029/2022rs007592

Bayliss, E. T. (1968). Design of monopulse antenna difference patterns with low sidelobes. *Bell System Technical Journal*, *47*(5), 623–650. https://doi.org/10.1002/j.1538-7305.1968.tb00056.x

Bracewell, R. N. (1999). *The Fourier transform & its applications* (pp. 11–12). McGraw-Hill Publishing Company.

Bucci, O. M., D'Urso, M., & Isernia, T. (2005). Optimal synthesis of difference patterns subject to arbitrary sidelobe bounds by using arbitrary array antennas. *IEE Proceedings Microwaves, Antennas and Propagation*, *152*(3), 129. https://doi.org/10.1049/ip-map:20045073

Bucci, O. M., Gennarelli, C., & Savarese, C. (1998). Representation of electromagnetic fields over arbitrary surfaces by a finite and nonredundant number of samples. *IEEE Transactions on Antennas and Propagation*, *46*(3), 351–359. https://doi.org/10.1109/8.662654

Bucci, O. M., Isernia, T., & Morabito, A. F. (2009). Optimal synthesis of directivity constrained pencil beams by means of circularly symmetric aperture fields. *IEEE Antennas and Wireless Propagation Letters*, *8*, 1386–1389. https://doi.org/10.1109/lawp.2009.2039189

Bucci, O. M., Isernia, T., Morabito, A. F., Perna, S., & Pinchera, D. (2009). Aperiodic arrays for space applications: An effective strategy for the overall design. In *European conference on antennas and propagation* (pp. 1–4). Retrieved from https://ieeexplore.ieee.org/document/5068016

Bucci, O. M., Isernia, T., Morabito, A. F., Perna, S., & Pinchera, D. (2010). Density and element-size tapering for the design of arrays with a reduced number of control points and high efficiency. In *European conference on antennas and propagation* (pp. 1–4). Retrieved from https://ieeexplore.ieee.org/document/5505377

Bui, L. T. P., Anselmi, N., Battaglia, G. M., Isernia, T., Rocca, P., & Morabito, A. F. (2021). Synthesis of wideband reconfigurable array antennas for monopulse radar applications. *Progress in Electromagnetics Research M*, *106*, 179–189. https://doi.org/10.2528/pierm21090905

Elliott, R. (1976). Design of line source antennas for difference patterns with sidelobes of individually arbitrary heights. *IEEE Transactions on Antennas and Propagation*, *24*(3), 310–316. https://doi.org/10.1109/tap.1976.1141343

Fan, X., Liang, J., Zhao, X., Zhang, Y., & So, H. C. (2020). Optimal synthesis of sum and difference beam patterns with a common weight vector for symmetric and asymmetric antenna arrays. *IEEE Transactions on Antennas and Propagation*, *68*(10), 6982–6996. https://doi.org/10.1109/tap.2020.2992860

Ferrando-Rocher, M., Herranz-Herruzo, J. I., Valero-Nogueira, A., & Bernardo-Clemente, B. (2023). All-metal monopulse antenna array in the *Ka*-band with a comparator network combining ridge and Groove Gap waveguides. *IEEE Antennas and Wireless Propagation Letters*, *22*(6), 1381–1385. https://doi.org/10.1109/lawp.2023.3242369

Heidari, H., Rezaei, P., Kiani, S., & Taherinezhad, M. (2023). A monopulse array antenna based on SIW with circular polarization for using in tracking systems. *AEU-International Journal of Electronics and Communications*, *162*, 154563. https://doi.org/10.1016/j.aeue.2023.154563

Isernia, T., & Panariello, G. (1998). Optimal focusing of scalar fields subject to arbitrary upper bounds. *Electronics Letters*, *34*(2), 162. https://doi.org/10.1049/el:19980212

Kou, N., & Yu, S. (2022). Low sidelobe orbital angular momentum vortex beams based on modified Bayliss synthesis method for circular array. *IEEE Antennas and Wireless Propagation Letters*, *21*(5), 968–972. https://doi.org/10.1109/lawp.2022.3153392

Leonardi, O., Pavone, M., Sorbello, G., Morabito, A. F., & Isernia, T. (2014). Compact single-layer circularly polarized antenna for short-range communication systems. *Microwave and Optical Technology Letters*, *56*(8), 1843–1846. https://doi.org/10.1002/mop.28453

Li, M., Liu, Y., & Guo, Y. J. (2021). Design of sum and difference patterns by optimizing element rotations and positions for linear dipole array. *IEEE Transactions on Antennas and Propagation*, *69*(5), 3027–3032. https://doi.org/10.1109/tap.2020.3037764

Li, Q., Li, X., Qi, Z., Zhu, H., Huang, Y., Akram, Z., & Jiang, X. (2019). Pattern synthesis of the multimode orbital angular momentum beams based on the fruit fly optimization algorithm. *International Journal of RF and Microwave Computer-Aided Engineering*, *29*(10), e21876. https://doi.org/10.1002/mmce.21876

Li, Q., Qi, Z., Huang, Y., Zhu, H., Li, X., Li, X., & Jiang, X. (2018). Orbital angular momentum beams synthesis based on the fruit fly optimization algorithm. In *2018 IEEE Asia-pacific conference on antennas and propagation (APCAP)* (pp. 490–491). https://doi.org/10.1109/apcap.2018.8538113

McNamara, D. (1993). Direct synthesis of optimum difference patterns for discrete linear arrays using Zolotarev distributions. *IEE Proceedings H Microwaves, Antennas and Propagation*, *140*(6), 495. https://doi.org/10.1049/ip-h-2.1993.0081

Mohammadi, M., & Kashani, F. H. (2009). Planar eight port waveguide mono-pulse comparator. *Progress in Electromagnetics Research C*, *6*, 103–113. https://doi.org/10.2528/pierc08122805

Mohammadi, M., Kashani, F. H., & Ghalibafan, J. (2009). A compact planar monopulse combining network at W-band. https://doi.org/10.1109/ieeegcc.2009.5734259

Morabito, A. F., Di Carlo, A., Di Donato, L., Isernia, T., & Sorbello, G. (2019). Extending spectral factorization to array pattern synthesis including sparseness, mutual coupling, and mounting-platform effects. *IEEE Transactions on Antennas and Propagation*, *67*(7), 4548–4559. https://doi.org/10.1109/tap.2019.2905977

Morabito, A. F., Palmeri, R., Morabito, V. A., Laganà, A. R., & Isernia, T. (2019). Single-surface phaseless characterization of antennas via hierarchically ordered optimizations. *IEEE Transactions on Antennas and Propagation*, *67*(1), 461–474. https://doi.org/10.1109/tap.2018.2877270

Morabito, A. F., & Rocca, P. (2010). Optimal synthesis of sum and difference patterns with arbitrary sidelobes subject to common excitations constraints. *IEEE Antennas and Wireless Propagation Letters*, *9*, 623–626. https://doi.org/10.1109/lawp.2010.2053832

Palmeri, R., Isernia, T., & Morabito, A. F. (2019). Diagnosis of planar arrays through phaseless measurements and sparsity promotion. *IEEE Antennas and Wireless Propagation Letters*, *18*(6), 1273–1277. https://doi.org/10.1109/lawp.2019.2914529

Qin, Y., Liu, K., Cheng, Y., Li, X., Wang, H., & Gao, Y. (2017). Sidelobe suppression and beam collimation in the generation of vortex electromagnetic waves for radar imaging. *IEEE Antennas and Wireless Propagation Letters*, *16*, 1289–1292. https://doi.org/10.1109/lawp.2016.2633008

Rocca, P., & Morabito, A. F. (2015). Optimal synthesis of reconfigurable planar arrays with simplified architectures for monopulse radar applications. *IEEE Transactions on Antennas and Propagation*, *63*(3), 1048–1058. https://doi.org/10.1109/TAP.2014.2386359

Sherman, S. R. (1984). Monopulse principles and techniques. Retrieved from http://ci.nii.ac.jp/ncid/BA23959856

Shirkolaei, M. M., & Ghalibafan, J. (2021). Magnetically scannable slotted waveguide antenna based on the ferrite with gain enhancement. In *Waves in random and complex media* (pp. 1–11). https://doi.org/10.1080/17455030.2021.1983234

Shirkolaei, M. M., & Jafari, M. (2020). A new class of wideband microstrip falcate patch antennas with reconfigurable capability at circular-polarization. *Microwave and Optical Technology Letters*, *62*(12), 3922–3927. https://doi.org/10.1002/mop.32529

Yu, S., & Kou, N. (2022). Synthesis for OAM vortex electromagnetic waves based on Fourier–Bessel expansion. *IEEE Transactions on Antennas and Propagation*, *71*(2), 1539–1547. https://doi.org/10.1109/tap.2022.3225587